

Modulating Electronic Structure of PtCo-Pt_{rich} Nanowires with Ru atoms for Boosted Hydrogen Evolution Catalysis

Xianjun Cao, Li Gao, Junpeng Qu, Lu Li, Yuhan Xie, Yufei Zhao,* Guoxiu Wang,* and Hao Liu*

Rational design and development of highly efficient hydrogen evolution reaction (HER) electrocatalysts is of great significance for the development of green water electrolysis hydrogen production technology. Ru-engineered 1D PtCo-Pt_{rich} nanowires (Ru-Pt_{rich}Co NWs) are fabricated by a facile electrodeposition method. The rich Pt surface on 1D Pt₃Co contributes to the fully exposed active sites and enhanced intrinsic catalytic activity (co-engineered by Ru and Co atoms) for HER. The incorporation of Ru atoms can not only accelerate the water dissociation in alkaline condition to provide sufficient H^{*} but also modulate the electronic structure of Pt to achieve optimized H^{*} adsorption energy. As a result, Ru-Pt_{rich}Co NWs have exhibited ultralow HER overpotentials (η) of 8 and 112 mV to achieve current densities of 10 and 100 mA cm⁻² in 1 M KOH, respectively, which far exceed those of commercial Pt/C catalyst ($\eta_{10} = 29$ mV, $\eta_{100} = 206$ mV). Density functional theory (DFT) calculations further demonstrate that the incorporated Ru atoms possess strong water adsorption capacity (-0.52 vs -0.12 eV for Pt), facilitating water dissociation. The Pt atoms in the outermost Pt-rich skin of Ru-Pt_{rich}Co NWs achieve optimized H^{*} adsorption free energy (ΔG_{H^*}) of -0.08 eV, boosting hydrogen generation.

1. Introduction


Issues such as the depletion of fossil fuels and global warming caused by excessive carbon emissions have attracted widespread attention. Under the strategy of sustainable development, hydrogen energy is considered as the most ideal green and clean energy, which possesses a high combustion calorific value and produces water with no carbon emissions.^[1-4] At present, electrochemical water splitting for hydrogen production has been regarded as one of the most promising and sustainable ways. Thus, it is of great importance to develop high-performance hydrogen evolution electrocatalysts to reduce the energy loss in water electrolysis. Metallic Pt shows suitable H^{*} binding energy, which has been considered as benchmark hydrogen evolution reaction (HER) electrocatalyst.^[5-7] Introducing other metal elements to Pt catalysts can reduce the amount of precious metals and ensure high catalytic efficiency, which

effectively balances the cost and catalytic activity. In addition, fully exposing the active ingredients to the outer surface of the catalysts is also one of the strategies to achieve the accelerated catalytic activity.^[8] Therefore, it is great significance to rationally design the structure and composition of Pt-based catalysts.

Since alkaline HER requires additional water splitting to generate H^{*}, this makes alkaline HER consume more energy than acidic HER, thus inhibiting the reaction rate.^[9-11] Therefore, in alkaline HER, both water dissociation and the H^{*} adsorption on active sites determine the overall reaction rate. It has been reported that introducing transition metals (Co, Fe, Ni, etc.) into Pt to form alloy can effectively adjust d-band center of Pt and inhibit the formation of Pt oxides, which can not only optimize the adsorption strength HER active intermediates, but also ensure the stable existence of Pt active sites, thus achieving boosted HER catalytic activity.^[12,13] In addition, it is found that the metal Ru species showed strong ability to capture water molecules in alkaline electrolyte.^[14,15] Therefore, the introduction of metal Ru into Pt-based nanomaterials can facilitate rapid water dissociation and thus accelerate alkaline HER.

Except for the composition, the nanostructure of Pt-based catalysts also has vital influence on the HER catalytic capability. For instance, the construction of 1D structure can effectively inhibit adverse reactions such as agglomeration and dissolution, and

X. Cao, L. Gao, J. Qu, L. Li, Y. Zhao
Joint International Laboratory on Environmental and Energy Frontier
Materials
School of Environmental and Chemical Engineering
Shanghai University
Shanghai 200444, P. R. China
E-mail: yufei-zhao@shu.edu.cn
Y. Xie, G. Wang, H. Liu
Centre for Clean Energy Technology
Faculty of Science
University of Technology Sydney
Broadway, Sydney, NSW 2007, Australia
E-mail: Guoxiu.Wang@uts.edu.au; hao.liu@uts.edu.au

 The ORCID identification number(s) for the author(s) of this article can be found under <https://doi.org/10.1002/sml.202302639>

© 2023 The Authors. Small published by Wiley-VCH GmbH. This is an open access article under the terms of the Creative Commons Attribution-NonCommercial License, which permits use, distribution and reproduction in any medium, provided the original work is properly cited and is not used for commercial purposes.

DOI: 10.1002/sml.202302639

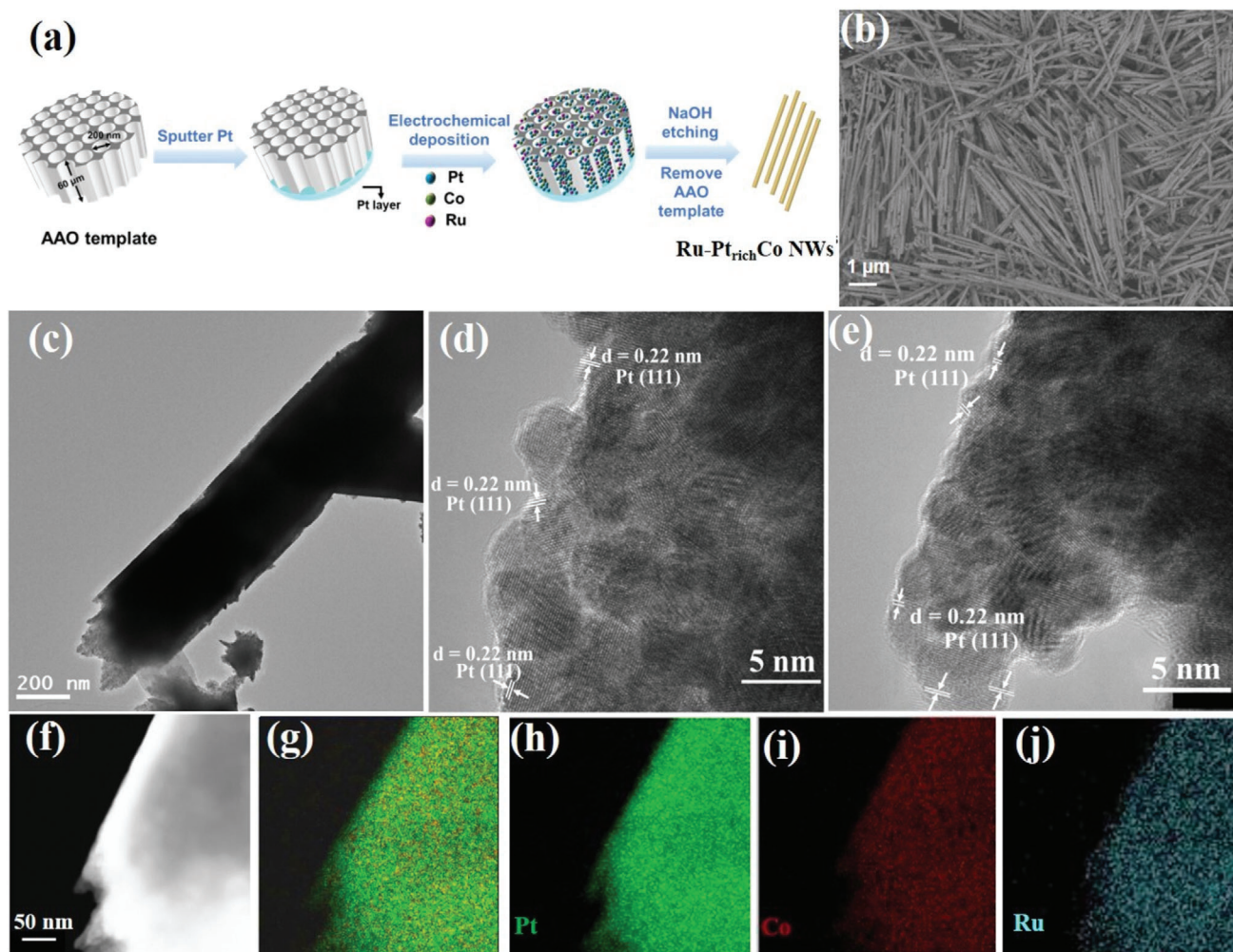


Figure 1. a) Schematic diagram of the preparation of Ru-Pt-richCo NWs. b) SEM image, c) TEM image, d,e) HR-TEM images and f–j) elemental EDX mapping.

accelerate the HER kinetics.^[16,17] Moreover, the atomic structure with more Pt atoms exposed also showed better HER catalytic capability.^[18,19] For example, subsurface Co in PtCo@Pt can induce a high proportion of (221) planes on the outer surface Pt as active sites, enabling PtCo/C NWs to achieve current density of 10 mA cm^{-2} at 32.7 mV overpotential for alkaline HER.^[20] Therefore, rational designing unique nanostructured HER electrocatalysts can lead to excellent catalytic performance.

Herein, we have designed basic HER electrocatalysts with 1D Pt-rich-skinned trimetallic Ru-Pt_{rich}Co nanowires (Ru-Pt_{rich}Co NWs) by one-step electrodeposition assisted by anodized aluminum oxide (AAO) templates. The abundant Pt surface provides a large number of active sites and the modulated electronic structure (co-engineered by Ru and Co atoms) facilitates the hydrogen evolution. The incorporated small amount of Ru not only promotes the adsorption and dissociation of water to continuously provides H^{*}, but also engineered surface Pt atoms to exhibit optimized H^{*} adsorption energy. The Ru-Pt_{rich}Co NWs exhibited excellent HER activity in alkaline electrolytes with overpotentials of 8 and 112 mV to achieve current densities of 10

and 100 mA cm^{-2} , respectively, which are much higher than the commercial Pt/C catalyst ($\eta_{10} = 29 \text{ mV}$, $\eta_{100} = 206 \text{ mV}$). Density functional theory (DFT) calculations results demonstrate that the Pt sites and Ru sites on the Ru-Pt_{rich}Co NWs (111) surface have exhibited optimized H^{*} adsorption free energy ($\Delta G_{\text{H}^*} = -0.08 \text{ eV}$) and strong H₂O adsorption capability, respectively (-0.52 eV), facilitating HER process in alkaline condition.

2. Results and Discussion

The fabrication process of Ru-Pt_{rich}Co NWs is shown in **Figure 1a**. 1D nanowire structures of Ru-Pt_{rich}Co NWs were synthesized by electrodeposition using AAO as hard templates. The standard electrochemical potentials of [PtCl₆]²⁻/Pt (0.74 V vs SHE) and Ru³⁺/Ru (0.6 V vs SHE) pairs are close to each other, which is quite different to that of Co²⁺/Co (-0.28 V vs SHE) pair.^[21–24] The metal ions of Pt and Ru can be reduced to metal Pt and Ru at a lower reduction potential (-0.35 V vs SCE), while Co needs to be reduced at a higher reduction potential (-1.00 V vs SCE).^[25,26]

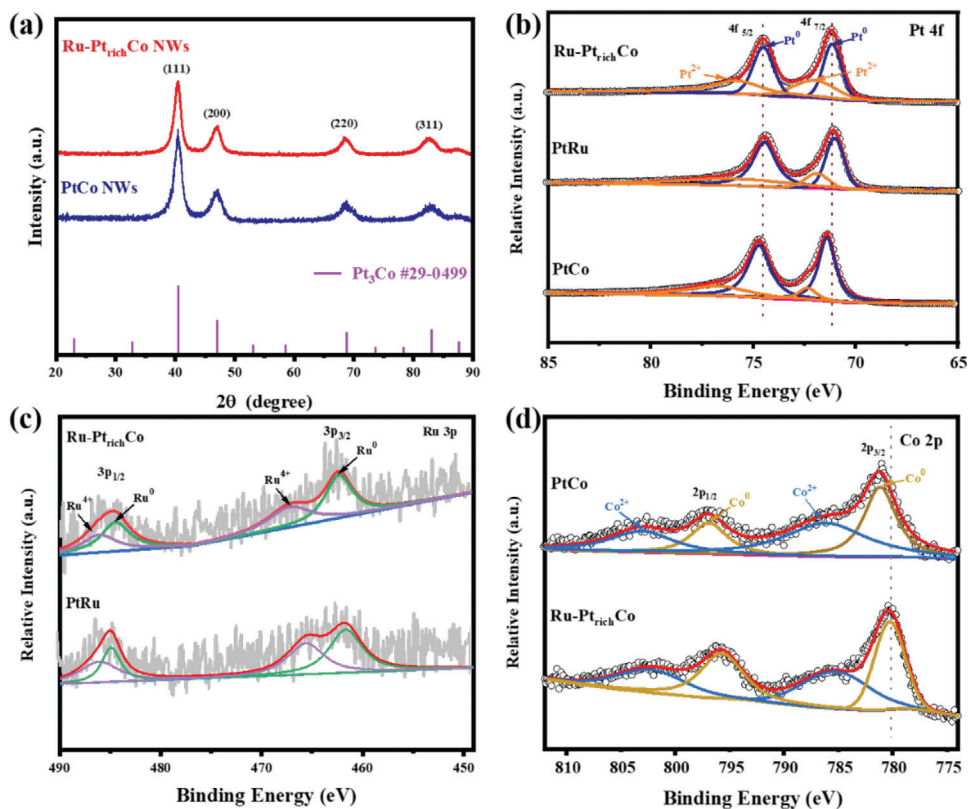


Figure 2. a) XRD pattern of PtCo and Ru-Pt_{rich}Co NWs. XPS spectra and deconvoluted peaks of Ru-Pt_{rich}Co, PtRu, and PtCo NWs in the regions of b) Pt 4f, c) Ru 3p, and d) Co 2p.

The scanning electron microscope (SEM) image of Ru-Pt_{rich}Co NWs is shown in Figure 1b, which shows a typical 1D nanowires with length of 9–10 μm . Bimetallic PtCo, PtRu, and CoRu NWs also show similar nanowire structures (Figure S2, Supporting Information). Transmission electron microscope (TEM) image in Figure 1c confirms that the diameter of Ru-Pt_{rich}Co NWs is close to the pore size of AAO template, which is ≈ 200 nm. The uniform 1D nanowire structure of Ru-Pt_{rich}Co NWs not only enhances the electron transfer capability, but also increases the interaction with the reactants/intermediates.^[27] The high-resolution TEM (HR-TEM) images (Figure 1d,e) showed the lattice fringe spacing at the edge of the nanowire is ≈ 0.22 nm, corresponding to the (111) plane of metallic Pt, demonstrating a Pt-rich skin structure on the surface of Ru-Pt_{rich}Co NWs. Furthermore, elemental distributions of Ru-Pt_{rich}Co NWs in Figure 1f–j show a homogenous distribution of Pt, Co, and Ru along the nanowire. Specifically, a clear Pt profile on the edge of Ru-Pt_{rich}Co NWs has been observed, while almost no Co profile distributed at the edge sites, which further confirms the enrichment of Pt on the surface of nanowires. This is consistent with the energy dispersive X-ray (EDX) line scan results (Figure S3, Supporting Information). Furthermore, the atomic ratio of Pt/Co/Ru in Ru-Pt_{rich}Co NWs was determined to be 14/5/1 by EDX and inductively coupled plasma optical emission spectrometer (ICP-OES).

Figure 2a are the X-ray diffraction (XRD) patterns of Ru-Pt_{rich}Co NWs and PtCo NWs, which shows a typical face-centered cubic (fcc) structure. The dominant peaks of Ru-Pt_{rich}Co NWs and

PtCo NWs are identified at 40.5°, 47.1°, 68.8°, and 83.0° assigned to the (111), (200), (220), and (311) planes (JCPDS 29–0499) of Pt₃Co, indicating the crystal structure of Ru-Pt_{rich}Co NWs has not been affected by the incorporation of Ru due to the low content property (2 wt.%).^[28] In addition, the XRD diffraction peaks of bimetallic PtRu NWs prepared by electrodeposition method are consistent with those of metallic Pt (JCPDS 87–0647) without obvious peak shift (Figure S4, Supporting Information). The surface electronic states and compositions of Ru-Pt_{rich}Co NWs, PtRu NWs, and PtCo NWs have been identified by the X-ray photoelectron spectroscopy (XPS). The full spectrum shows that the elements of Ru-Pt_{rich}Co NWs are Pt, Co, and Ru (Figure S5, Supporting Information). The Pt 4f of Ru-Pt_{rich}Co, PtRu and PtCo NWs all contain Pt 4f_{5/2} and Pt 4f_{7/2} doublets located at 74.49, 71.17, 74.37, 71.05 and 74.73, 71.41 eV, respectively (Figure 2b). The binding energy of Pt 4f in Ru-Pt_{rich}Co NWs is close to that of PtRu NWs (around 0.1 eV shift), but much obvious shift has been observed for PtCo NWs (≈ 0.3 eV shift), indicating that the outer surface of Ru-Pt_{rich}Co NWs is mainly composed of Ru engineered platinum-rich skin structure. The XPS analysis of Ru 3p and Co 2p in Figure 2c,d shows that Ru and Co in Ru-Pt_{rich}Co, PtRu, and PtCo NWs are presented as Ru⁰, Ru⁴⁺, and Co⁰, Co²⁺, respectively. The slightly peak shifts of Ru and Co are caused by the interaction of the three metals, demonstrating the strong electronic interactions between Pt, Co, and Ru atoms in Ru-Pt_{rich}Co NWs, which effectively tunes the d-band center of active sites to optimize the H₂O and H⁺ adsorption energy.^[29] Moreover, the dominant

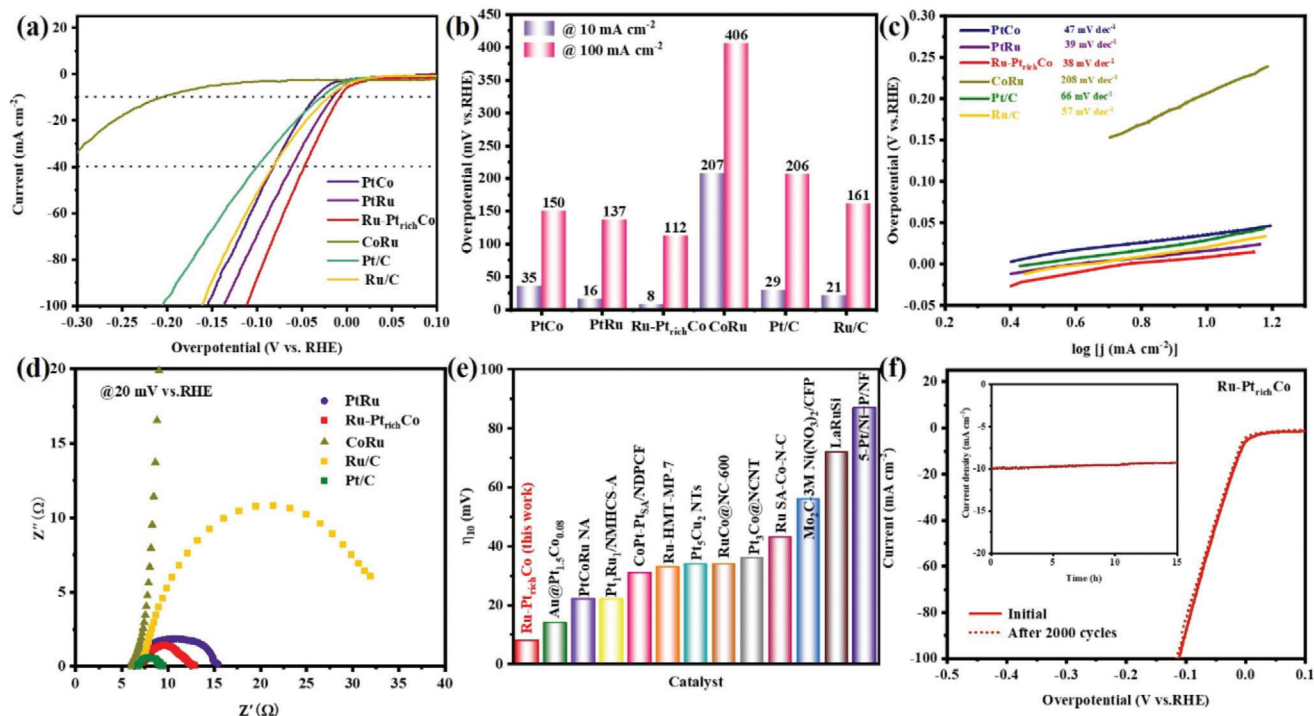


Figure 3. HER activity. a) LSV curves, b) overpotentials at current densities of 10 and 100 mA cm⁻², c) Tafel plots, d) EIS spectra of different electrocatalysts in 1 M KOH. e) The comparison of overpotential at 10 mA cm⁻² between Ru-Pt_{rich}Co NWs and recently reported HER electrocatalysts. f) The polarization curves are recorded before and after 2000 cycles of Ru-Pt_{rich}Co NWs. Inset is the chronoamperometry at an overpotential of 10 mA cm⁻² in 1 M KOH.

zero-valence metal state of Pt, Co, and Ru in the designed catalysts are also beneficial for HER.^[30]

The alkaline (1 M KOH) HER activities of PtCo, PtRu, Ru-Pt_{rich}Co NWs, reference Pt/C (20 wt.%) and reference Ru/C (40 wt.%) were evaluated by linear sweep voltammetry (LSV) in a three-electrode system (Figure 3a). The overpotentials of PtCo and PtRu NWs at 10 and 100 mA cm⁻² current densities are 35, 150 and 16, 137 mV, respectively, which are close to those of benchmark catalysts of Ru/C (29 mV) and commercial Pt/C (21 mV). The above results suggest that the Pt sites in PtCo and PtRu NWs play a key role for boosted alkaline HER activity. Further introducing Ru into PtCo NWs forming Ru-Pt_{rich}Co NWs, the overpotential of HER is further reduced to $\eta_{10} = 8$ and $\eta_{100} = 112$ mV, which is much superior compared to that of references Ru/C and Pt/C (29 and 21 mV). This may attribute to the effective engineering electronic structure of surface Pt atoms by both of Co and Ru atoms, thereby further reducing the overpotential for HER. The remarkable electrocatalytic performance of Ru-Pt_{rich}Co NWs also exceeds other previously reported HER electrocatalysts in alkaline conditions (Figure 3e; Table S1, Supporting Information).^[31–42] The electrochemically active specific surface area (ECSA) has been evaluated by integrating the charge of the H adsorption/desorption region by cyclic voltammetry (Figure S6, Supporting Information). The ECSA of Ru-Pt_{rich}Co NWs (97.13 m² g⁻¹) is much higher than that of commercial Pt/C (62.23 m² g⁻¹), resulting in superior HER performance. Tafel slopes are obtained from the LSV results in Figure 3c.^[43] It is

found that the Tafel slope of Pt_{rich}Co NWs (38 mV dec⁻¹) is the smallest compared with PtRu NWs (39 mV dec⁻¹), PtCo NWs (47 mV dec⁻¹), Ru/C (57 mV dec⁻¹), and Pt/C (66 mV dec⁻¹), attributing to the co-engineering strategy of Ru and Co promoting the water dissociation and H* adsorption, thereby accelerating the kinetic process of Ru-Pt_{rich}Co NWs.^[44] The electrochemical impedance spectroscopy (EIS) was used to evaluate the charge transfer capability at the catalyst-electrolyte interface. The smaller the charge transfer resistance (R_{ct}), the better the catalytic performance.^[45] At the overpotential of 20 mV, Ru-Pt_{rich}Co NWs have exhibited the smallest R_{ct} (≈ 6 Ω), suggesting that Ru-Pt_{rich}Co NWs possess much faster electron transfer rate than other comparison materials.

The stability of Ru-Pt_{rich}Co NWs is also an important parameter to evaluate the corresponding alkaline HER performance, which can be tested by cyclic voltammetry (CV) and chronoamperometry. It is worth noting that after 2000 cycles CV accelerated durability tests, the LSV curve of Ru-Pt_{rich}Co NWs does not change significantly and the overpotential change is negligible (Figure 3f). In addition, the chronoamperometry test was performed at the current density of 10 mA cm⁻² for 15 h, and the current density remain basically stable with only a decrease of 7.68% (inset of Figure 3f). The excellent stability of Ru-Pt_{rich}Co can be attributed to the fact that the surface Pt-rich skin structure inhibits the leaching of transition metal Co, and the charge transfer between Pt, Co, and Ru inhibits the further oxidation of surface Pt. The SEM image of Ru-Pt_{rich}Co NWs after the durability

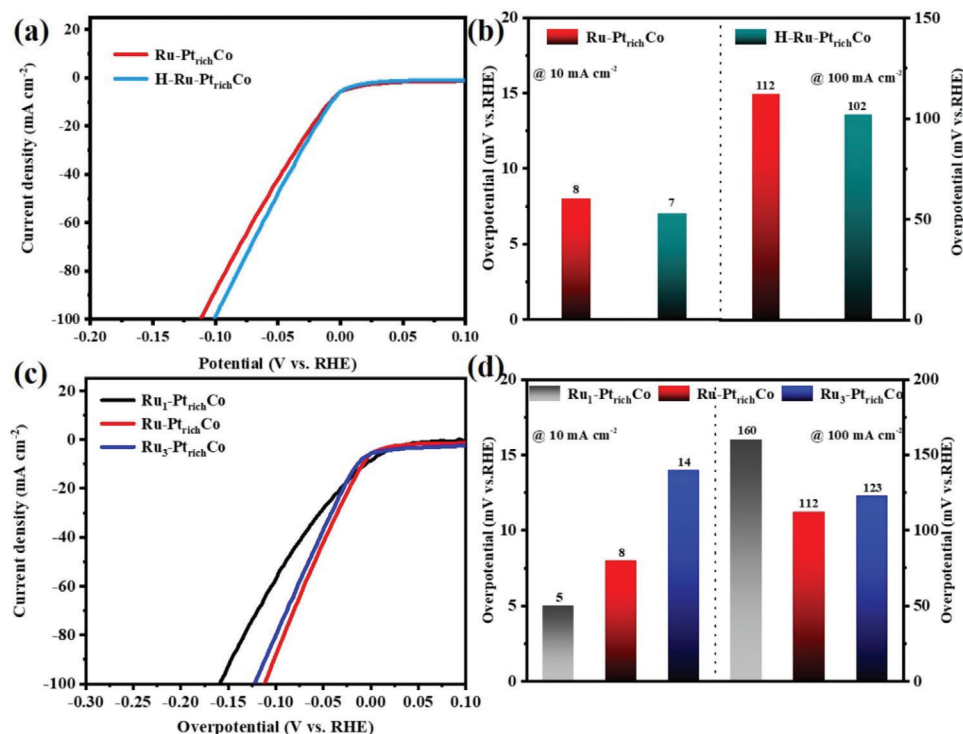


Figure 4. a) Polarization curve, b) overpotentials at current densities of 10 and 100 mA cm⁻² of Ru-Pt_{rich}Co and H-Ru-Pt_{rich}Co NWs in 1 M KOH. c) polarization curve, d) overpotentials at current densities of 10 and 100 mA cm⁻² of Ru₁-Pt_{rich}Co, Pt-PtCoRu, and Ru₃-Pt_{rich}Co NWs in 1 M KOH.

test (Figure S7, Supporting Information) also show that there is no obvious morphology change during HER process, further confirming the stability property.

To further verify the Pt-rich skin structure on the outer surface of Ru-Pt_{rich}Co NWs, Ru-Pt_{rich}Co NWs have been soaked in 0.5 M H₂SO₄ for 2.5 h to obtain H-Ru-Pt_{rich}Co NWs. The SEM image of H-Ru-Pt_{rich}Co NWs demonstrates that the morphology of Ru-Pt_{rich}Co NWs has almost no change before and after acid treatment (Figure S8, Supporting Information). Moreover, the overpotentials of H-Ru-Pt_{rich}Co NWs at current densities of 10 and 100 mA cm⁻² are 7 and 102 mV for alkaline HER, respectively (Figure 4a,b), which are quite close to the HER performance of Ru-Pt_{rich}Co NWs, further verifying that the surface of Ru-Pt_{rich}Co NWs is a Pt-rich skin structure, and Co atoms are mainly distributed inside of the nanowires. In addition, in order to explore the effect of Ru on the catalytic performance of Ru-Pt_{rich}Co NWs for alkaline HER, different amount of Ru precursors (1, 2, and 3 mM RuCl₃) were introduced to obtain Ru₁-Pt_{rich}Co, Ru₂-Pt_{rich}Co (the aforementioned Ru-Pt_{rich}Co NWs) and Ru₃-Pt_{rich}Co NWs. The XRD spectra and SEM images of Ru₁-Pt_{rich}Co and Ru₃-Pt_{rich}Co NWs in Figures S9 and S10 (Supporting Information) show the well-crystallized and uniform nanowire structures, similar to that of Ru-Pt_{rich}Co NWs. The LSV results show that Ru₁-Pt_{rich}Co NWs and Ru₃-Pt_{rich}Co NWs have achieved current densities of 10 and 100 mA cm⁻² at the overpotential of 5, 160 and 14, 123 mV, respectively (Figure 4c,d). Ru₁-Pt_{rich}Co NWs have smaller overpotentials at low current densities, but higher overpotentials than Ru-Pt_{rich}Co NWs at higher current densities. Therefore, Ru incorporation does have a vital influ-

ence on the HER catalytic activity of Pt_{rich}Co and Ru-Pt_{rich}Co NWs with moderate Ru doping amount (2 mM) exhibit the best performance.

To gain a deeper understanding of the enhanced activity of Ru-Pt_{rich}Co NWs for alkaline HER, we have calculated the adsorption energies of active intermediates H* and H₂O on the surface of Ru-Pt_{rich}Co NWs (111) by density functional theory (Figure 5a-c). Figures S11–S14 (Supporting Information) show the atomic distribution maps of H* and H₂O adsorption on Pt and Ru sites on Ru-Pt_{rich}Co NWs (111), respectively. In HER, moderate H* adsorption free energy ($\Delta G_{H^*} \approx 0$) can ensure fast H* adsorption and desorption capabilities.^[46] Figure 5d is the H* adsorption free energy diagram for Pt and Ru sites on the surface of Ru-Pt_{rich}Co NWs (111). The calculated results show that the ΔG_{H^*} of Pt sites on Ru-Pt_{rich}Co NWs (111) is -0.08 eV, which is closer to zero than the ΔG_{H^*} (-0.13 eV) for Ru sites. Therefore, Pt on the surface of Ru-Pt_{rich}Co NWs is the optimal H* adsorption site during HER process. In alkaline electrolytes, the lack of free protons severely hinders HER. Thus, the water dissociation ability to generate H* is also an important parameter to determine the HER activity. The adsorption energy of water is usually used to judge the ability of water to dissociate into OH⁻ and H*.^[47] As shown in Figure 5e, the water adsorption energy of Ru sites (-0.52 eV) on Ru-Pt_{rich}Co NWs (111) is much lower than that of Pt sites (-0.12 eV). This indicates that water molecules will preferentially adsorb on the Ru sites on the surface of Ru-Pt_{rich}Co NWs. The above DFT calculation analysis shows that in the alkaline electrolyte, the Ru atoms on the surface of Ru-Pt_{rich}Co NWs enhance the water adsorption and dissociation, and the generated

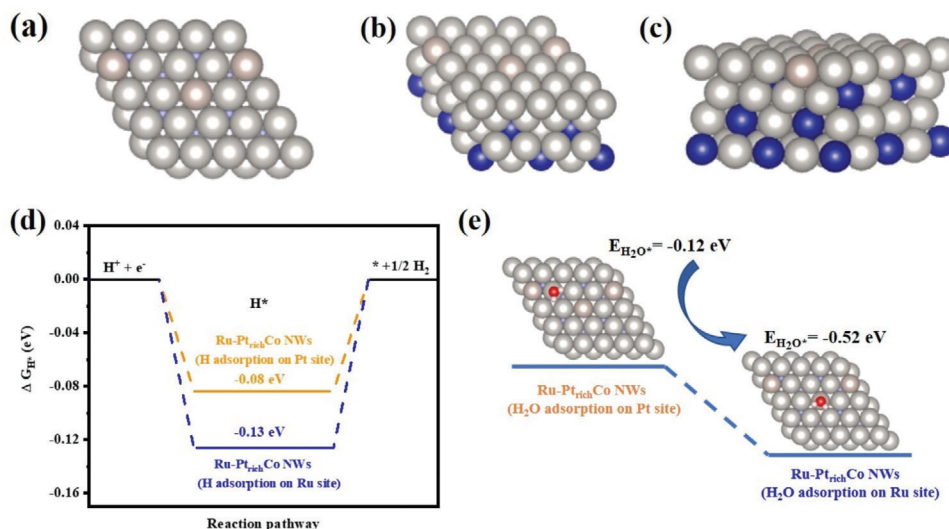


Figure 5. a) Top, b) side, and c) front side view of Ru-Pt_{rich}Co NWs (111). Gray, light pink, and blue balls represent Pt, Ru, and Co atoms, respectively. d) H^{*} adsorption free energy and e) water adsorption energy calculated for Pt and Ru sites on Ru-Pt_{rich}Co NWs (111). White and red balls represent H and O atoms, respectively.

H^{*} quickly transfer to the adjacent Pt atoms with optimal H^{*} adsorption energy, thus accelerating the entire HER process.

To investigate the application potential of Ru-Pt_{rich}Co in overall water splitting (OWS), a two-electrode water electrolyzer has been assembled using Ru-Pt_{rich}Co NWs and RuO₂ as cathode and anode, respectively, in 1 M KOH (Figure 6d). The polarization curves of Ru-Pt_{rich}Co||RuO₂ and reference Pt/C||RuO₂ (Figure 6a) show that Ru-Pt_{rich}Co||RuO₂ requires a low cell voltage of 1.580 V to drive a current density of 10 mA cm⁻², while Pt/C||RuO₂ requires 1.636 V. It is worth mentioned that the water splitting voltage of Ru-Pt_{rich}Co ||RuO₂ is also smaller than most of previously reported catalysts (Figure 6b; Table S2, Supporting Information).^[48–57] In addition, the current density of Ru-Pt_{rich}Co||RuO₂ water electrolyzer has no obvious decay after continuous operation for 15 h at a voltage of 1.6 V, which indicates that it possesses excellent durability for overall water splitting. In contrast, the current density of Pt/C||RuO₂ decays rapidly (Figure S15, Supporting Information). In conclusion, Ru-Pt_{rich}Co NWs are promising commercial prospects in water splitting applications.

3. Conclusion

In summary, PtCoRu alloy nanowire electrocatalysts with Pt-rich skin were prepared by alternating electrodeposition at different potentials. In alkaline electrolytes, Ru-Pt_{rich}Co NWs have exhibited overpotentials of 8 and 112 mV at current densities of 10 and 100 mA cm⁻², respectively, and also exhibited a small Tafel slope of 38 mV dec⁻¹, which is superior to commercial Pt/C, Ru/C and most HER electrocatalysts reported in recent years. Pt and Ru on the surface of Ru-Pt_{rich}Co NWs efficiently inhibit the leaching of transition metal Co and accelerate the water dissociation rate. The strong electronic modulation effect between the three metals further optimizes the adsorption energy of intermediates on Pt atoms. The high catalytic activity and stability of Ru-Pt_{rich}Co

NWs toward alkaline HER demonstrate the promising application prospects in overall water splitting technology.

4. Experimental Section

Reagents and Chemicals: Potassium chloroplatinate (K₂PtCl₆), Cobalt (II) sulfate heptahydrate (CoSO₄·7H₂O), Ruthenium (III) Chloride (RuCl₃), and Orthoboric acid (H₃BO₃) were purchased from Adamas. Sodium Hydroxide (NaOH) was purchased from Greagent. All reagents were of analytical reagent grade and used without further purification.

Synthesis of Ru-Pt_{rich}Co NWs: Ru-Pt_{rich}Co nanowires were prepared by electrochemical constant voltage electrodeposition using double-pass anodized aluminum oxide (AAO, 200 nm pore size, 60 nm thick, Puyuan Nano) as a template (Figure S1, Supporting Information). Before electrodeposition, a thin conductive layer was sprayed on the back of the AAO film as the working electrode, the platinum sheet electrode as the counter electrode, and Ag/AgCl as the reference electrode. The electrodeposition process was carried out with three electrodes in a single electrolytic cell at room temperature. The electrolyte was composed of 0.01 M K₂PtCl₆, 0.5 M CoSO₄·7H₂O, 2 mM RuCl₃, and deionized water. Adjust the pH of the solution to 3.5 with appropriate amount of boric acid and 0.1 M HCl solution. Alternately apply -1.00 V (vs SCE) and -0.35 V (vs SCE) for constant potential electrodeposition. After the electrodeposition, the AAO film was washed with a large amount of deionized water, and then the AAO was dissolved with 1 M NaOH to release the Ru-Pt_{rich}Co nanowires.

For comparison, under the same synthesis conditions, Ru₁-Pt_{rich}Co and Ru₃-Pt_{rich}Co NWs were obtained by changing the addition of RuCl₃ precursors in the electroplating solution to 1 and 3 mM, respectively.

Synthesis of Bimetallic Nanowires: The synthesis of PtCo, PtRu, and RuCo nanowires was similar to that of Ru-Pt_{rich}Co NWs, except that RuCl₃, CoSO₄·7H₂O, and K₂PtCl₆ were not added, respectively.

Characterization: The crystal structures of the prepared materials were characterized by X-ray diffraction (XRD, 3 KW D/MAX2200V). The morphology and microstructure of the samples were observed using a scanning electron microscope (SEM, JEOL JSM-7500F) and a transmission electron microscope (TEM, JEOL 2100F). Area and line scans were performed using energy dispersive X-ray spectroscopy (EDX) with JED 2300. X-ray photoelectron spectroscopy (XPS) analysis was performed on a Thermo Scientific K-Alpha. The content of metal elements in the material

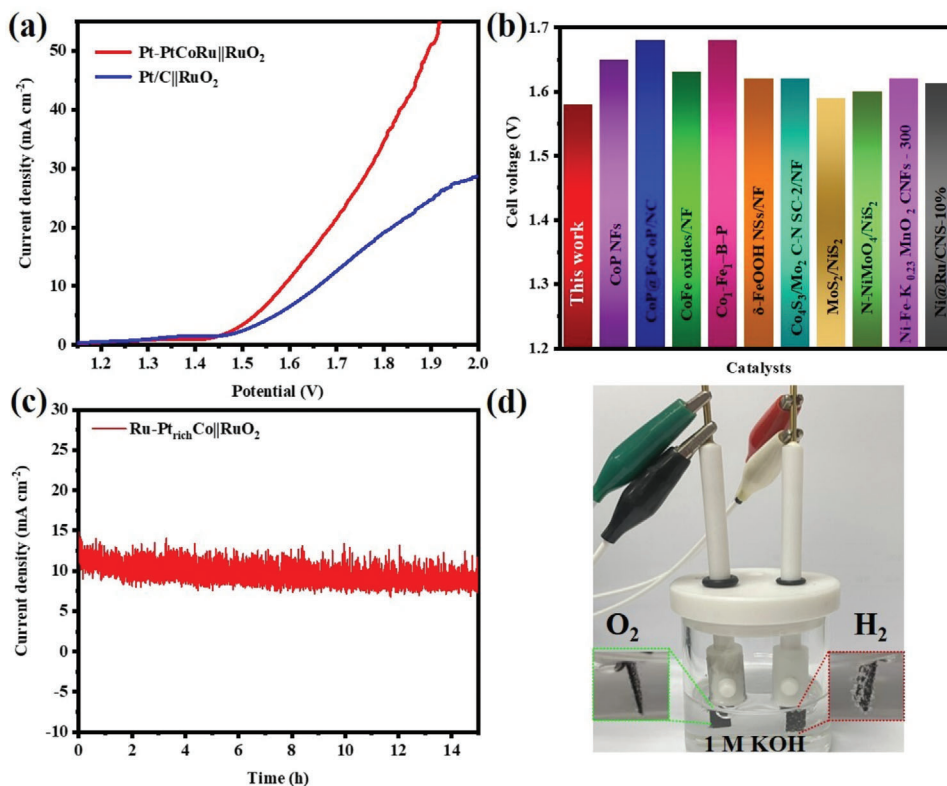


Figure 6. a) The polarization curves of Ru-Pt_{rich}Co ||RuO₂ and Pt/C||RuO₂ for overall water splitting, b) cell voltages of different catalysts for overall water splitting. c) Chronopotentiometry curves of Ru-Pt_{rich}Co ||RuO₂ water electrolysis at 1.6 V in 1 M KOH, d) diagram of the water splitting device, as the applied voltage increases, the bubbles of H₂ and O₂ on the cathode and anode gradually increase.

was detected by Agilent 5110 inductively coupled plasma optical emission spectrometer (ICP-OES).

Electrochemical Measurements: Electrochemical tests were performed using Pine electrochemical workstation in a three-electrode system. Glassy carbon rotating disk electrode (RDE, area: 0.196 cm²), Ag/AgCl (3.5 M KCl) and Pt wire electrode were used as working electrode, reference electrode, and counter electrode, respectively. Convert $E_{\text{Ag/AgCl}}$ to E_{RHE} by the Nernst equation:

$$E_{\text{RHE}} = E_{\text{Ag/AgCl}} + 0.059 * pH + 0.198 \quad (1)$$

Before electrochemical measurement, 1 mg sample, 1 mg Vulcan XC-72, 135 μL isopropanol, 15 μL ethanol, and 10 μL Nafion solution were placed in the sample tube, and black uniform ink was obtained after ultrasonication at room temperature for 2 h. Next, 15 μL of the above ink prepared on the newly polished RDE surface (loaded at 0.4778 mg cm⁻²). Subsequently, electrochemical tests were performed after standing to dry at room temperature for a few minutes. Linear sweep voltammetry (LSV) test was measured in 1.0 M KOH solution at a scan rate of 5 mV s⁻¹ and a spin rate of 1,600 rpm over the range of -0.3 to 0.1 V versus RHE. The electrochemically active specific surface area (ECSA) was measured by cyclic voltammetry (CV) test in 1 M KOH at a sweep rate of 50 mV s⁻¹. The electrochemical impedance spectroscopy (EIS) was performed on a CHI 660E electrochemical workstation with a recording frequency ranging from 0.01 to 10⁵ Hz, an amplitude of 5 mV and a voltage of 20 mV versus RHE. Here all potentials were iR compensated. The stability test adopts two electrochemical test methods of CV and chronoamperometry, respectively. The CV stability test was performed at -0.15 to 0.05 V versus RHE at a sweep rate of 50 mV s⁻¹ for 2000 cycles. After that, the electrodes obtained after 2000 cycles were used for LSV at a rate of 5 mV s⁻¹.

DFT Calculation: DFT calculations used the Vienna Ab initio Simulation Package (VASP) to calculate the binding energy for specific surfaces of catalysts.^[58] Projected augmented waves (PAW) and Perdew, Burke, and Ernzerhof (PBE) parameterized generalized exchange-correlation interactions are implemented by the VASP package.^[59,60] A cutoff energy of 400 eV was used in all calculations. A (3 × 3 × 2) Monkhorst-Pack *k*-point sampling were used for all surface calculations and boxes of 15 Å × 15 Å × 15 Å have been used for H₂O and H₂ calculation.

Supporting Information

Supporting Information is available from the Wiley Online Library or from the author.

Acknowledgements

This work was supported by Australia Research Council (FT180100705). Y.Z. thanks the support from Open Project of State Key Laboratory of Advanced Special Steel, the Shanghai Key Laboratory of Advanced Ferrometallurgy, Shanghai University (SKLASS 2021-**), "Joint International Laboratory on Environmental and Energy Frontier Materials" and "Innovation Research Team of High-Level Local Universities in Shanghai". Y.Z. also acknowledges the financial support from the National Natural Science Foundation of China (22209103).

Open access publishing facilitated by University of Technology Sydney, as part of the Wiley - University of Technology Sydney agreement via the Council of Australian University Librarians.

Conflict Of Interest

The authors declare no conflict of interest.

Data Availability Statement

The data that support the findings of this study are available in the supplementary material of this article.

Keywords

1D nanowires, hydrogen evolution reaction, Pt-rich skin, Ru engineering

Received: March 29, 2023

Revised: May 16, 2023

Published online: June 12, 2023

- [1] N. Tasnim Sahrin, K. Shiong Khoo, J. Wei Lim, R. Shamsuddin, F. Musa Ardo, H. Rawindran, M. Hassan, W. Kiatkittipong, E. Alaaeldin Abdelfattah, W. Da Oh, C. Kui Cheng, *Bioresour. Technol.* **2022**, 364, 128088.
- [2] F. Qureshi, M. Yusuf, H. Kamyab, D. V. N. Vo, S. Chelliapan, S. W. Joo, Y. Vasseghian, *Renew. Sust. Energ. Rev.* **2022**, 168, 112916.
- [3] T. Yusaf, L. Fernandes, A. R. Abu Talib, Y. S. Altarazi, W. Alrefae, K. Kadirgama, D. Ramasamy, A. Jayasuriya, G. Brown, R. Mamat, *Sustainability* **2022**, 14, 548.
- [4] J. Huo, X. Cao, Y. Tian, L. Li, J. Qu, Y. Xie, X. Nie, Y. Zhao, J. Zhang, H. Liu, *Nanoscale* **2023**, 15, 5448.
- [5] C. Li, J. B. Baek, *ACS Omega* **2019**, 5, 31.
- [6] A. Eftekhari, *Int. J. Hydrog. Energy* **2017**, 42, 11053.
- [7] J. Huo, Z. Shen, X. Cao, L. Li, Y. Zhao, H. Liu, G. Wang, *Small* **2022**, 18, 2202394.
- [8] S. Shen, Z. Wang, Z. Lin, K. Song, Q. Zhang, F. Meng, L. Gu, W. Zhong, *Adv. Mater.* **2022**, 34, 2110631.
- [9] A. H. Shah, Z. Zhang, Z. Huang, S. Wang, G. Zhong, C. Wan, A. N. Alexandrova, Y. Huang, X. Duan, *Nat. Catal.* **2022**, 5, 923.
- [10] N. Marković, B. Rgur, P. N. Ross, *J. Phys. Chem. B* **1997**, 101, 5405.
- [11] K. Seto, A. Iannelli, B. Love, J. Lipkowsky, *J. Electroanal. Chem. Interfacial Electrochem.* **1987**, 226, 351.
- [12] Y. Qin, X. Han, S. Gadipelli, J. Guo, S. Wu, L. Kang, J. Callison, Z. Guo, *J. Mater. Chem. A* **2019**, 7, 6543.
- [13] H. Zhai, G. Xu, J. Liu, T. Xu, C. Li, J. Bai, *Int. J. Hydrog. Energy* **2022**, 47, 2423.
- [14] B. Pang, X. Liu, T. Liu, T. Chen, X. Shen, W. Zhang, S. Wang, T. Liu, D. Liu, T. Ding, *Energ. Environ. Sci.* **2022**, 15, 102.
- [15] X. Cao, J. Huo, L. Li, J. Qu, Y. Zhao, W. Chen, C. Liu, H. Liu, G. Wang, *Adv. Energy Mater.* **2022**, 12, 2202119.
- [16] W. Yin, G. Zhang, X. Wang, H. Pang, *Adv. Colloid Interface Sci.* **2021**, 298, 102562.
- [17] X. Li, J. Wang, *InfoMat* **2020**, 2, 3.
- [18] X. Yin, L. Yang, Q. Gao, *Nanoscale* **2020**, 12, 15944.
- [19] J. Kang, X. Qiu, Q. Hu, J. Zhong, X. Gao, R. Huang, C. Wan, L.-M. Liu, X. Duan, L. Guo, *Nat. Catal.* **2021**, 4, 1050.
- [20] E. B. Tetteh, C. Gyan Barimah, H. Y. Lee, T. H. Kang, S. Kang, S. Ringe, J. S. Yu, *ACS Appl. Mater. Interfaces* **2022**, 14, 25246.
- [21] Ç. Üzümlü, T. Shahwan, A. E. Eroğlu, I. Lieberwirth, T. B. Scott, K. R. Hallam, *Chem. Eng. J.* **2008**, 144, 213.
- [22] X. Gu, X. Cong, Y. Ding, *ChemPhysChem* **2010**, 11, 841.
- [23] K. Gao, Y. Wang, Z. Wang, Z. Zhu, J. Wang, Z. Luo, C. Zhang, X. Huang, H. Zhang, W. Huang, *Chem. Commun.* **2018**, 54, 4613.
- [24] J. Wang, Y. Yuan, K. Ren, B. Wang, Z. Li, *J. Catal.* **2022**, 417, 178.
- [25] J. R. Choi, S. J. Oh, H. Ju, J. Cheon, *Nano Lett.* **2005**, 5, 2179.
- [26] Y. K. Su, D. H. Qin, H. L. Zhang, H. Li, H. L. Li, *Chem. Phys. Lett.* **2004**, 388, 406.
- [27] H. Huang, L. Fu, W. Kong, H. Ma, X. Zhang, J. Cai, S. Wang, Z. Xie, S. Xie, *Small* **2022**, 18, 2201333.
- [28] K. Ji, M. Xu, S.-M. Xu, Y. Wang, R. Ge, X. Hu, X. Sun, H. Duan, *Angew. Chem., Int. Ed.* **2022**, 61, e202209849.
- [29] J. Chen, G. Qian, H. Zhang, S. Feng, Y. Mo, L. Luo, S. Yin, *Adv. Funct. Mater.* **2022**, 32, 2107597.
- [30] C. Zhang, X. Liang, R. Xu, C. Dai, B. Wu, G. Yu, B. Chen, X. Wang, N. Liu, *Adv. Funct. Mater.* **2021**, 31, 2008298.
- [31] S. Battiato, L. Bruno, A. Terrasi, S. Mirabella, *ACS Appl. Energy Mater.* **2022**, 5, 2391.
- [32] W. Yang, P. Cheng, Z. Li, Y. Lin, M. Li, J. Zi, H. Shi, G. Li, Z. Lian, H. Li, *Adv. Funct. Mater.* **2022**, 32, 2205920.
- [33] S. Shen, Z. Hu, H. Zhang, K. Song, Z. Wang, Z. Lin, Q. Zhang, L. Gu, W. Zhong, *Angew. Chem., Int. Ed. Engl.* **2022**, 61, 202206460.
- [34] W. Zhao, C. Luo, Y. Lin, G. B. Wang, H. M. Chen, P. Kuang, J. Yu, *ACS Catal.* **2022**, 12, 5540.
- [35] L. Zhang, Z. Hu, J. Huang, Z. Chen, X. Li, Z. Feng, H. Yang, S. Huang, R. Luo, *J. Adv. Ceram.* **2022**, 11, 1294.
- [36] R. Wan, M. Luo, J. Wen, S. Liu, X. Kang, Y. Tian, *J. Energy Chem.* **2022**, 69, 44.
- [37] Y. Tong, J. Liu, L. Wang, B. J. Su, K. H. Wu, J. Y. Juang, F. Hou, L. Yin, S. X. Dou, J. Liu, J. Liang, *Adv. Funct. Mater.* **2022**, 32, 2205654.
- [38] S. L. Zhang, X. F. Lu, Z. P. Wu, D. Luan, X. W. D. Lou, *Angew. Chem., Int. Ed. Engl.* **2021**, 60, 19068.
- [39] H. Y. Chen, H. J. Niu, X. Ma, J. J. Feng, X. Weng, H. Huang, A. J. Wang, *J. Colloid Interface Sci.* **2020**, 561, 372.
- [40] F. Zhang, Y. Zhu, Y. Chen, Y. Lu, Q. Lin, L. Zhang, S. Tao, X. Zhang, H. Wang, *J. Mater. Chem. A* **2020**, 8, 12810.
- [41] Y. Zhao, X. Zhang, Y. Gao, Z. Chen, Z. Li, T. Ma, Z. Wu, L. Wang, S. Feng, *Small* **2022**, 18, 2105168.
- [42] H. Zhang, X. Guo, W. Liu, D. Wu, D. Cao, D. Cheng, *J. Colloid Interface Sci.* **2023**, 629, 53.
- [43] Y. Zhu, H. A. Tahini, Y. Wang, Q. Lin, Y. Liang, C. M. Doherty, Y. Liu, X. Li, J. Lu, S. C. Smith, C. Selomulya, X. Zhang, Z. Shao, H. Wang, *J. Mater. Chem. A* **2019**, 7, 14222.
- [44] Z. Cao, F. Dong, J. Pan, W. Xia, J.-G. Hu, X. Xu, *ACS Appl. Energy Mater.* **2022**, 5, 1496.
- [45] Y. L. Wu, X. Li, Y. S. Wei, Z. Fu, W. Wei, X. T. Wu, Q. L. Zhu, Q. Xu, *Adv. Mater.* **2021**, 33, 2006965.
- [46] R. Subbaraman, D. Tripkovic, D. Strmcnik, K. C. Chang, M. Uchiumura, A. P. Paulikas, V. Stamenkovic, N. M. Markovic, *Science* **2011**, 334, 1256.
- [47] Q. Ju, R. Ma, Y. Pei, B. Guo, Z. Li, Q. Liu, T. Thomas, M. Yang, G. J. Hutchings, J. Wang, *Adv. Energy Mater.* **2020**, 10, 2000067.
- [48] J. Shi, F. Qiu, W. Yuan, M. Guo, Z. H. Lu, *Chem. Eng. J.* **2021**, 403, 126312.
- [49] Y. Liu, X. Luo, C. Zhou, S. Du, D. Zhen, B. Chen, J. Li, Q. Wu, Y. Iru, D. Chen, *Appl. Catal. B* **2020**, 260, 118197.
- [50] H. Liao, X. Guo, Y. Hou, H. Liang, Z. Zhou, H. Yang, *Small* **2020**, 16, 1905223.
- [51] Z. Wu, D. Nie, M. Song, T. Jiao, G. Fu, X. Liu, *Nanoscale* **2019**, 11, 7506.
- [52] W. Wu, Y. Wu, D. Zheng, K. Wang, Z. Tang, *Electrochim. Acta.* **2019**, 320, 134568.
- [53] J. Lin, P. Wang, H. Wang, C. Li, X. Si, J. Qi, J. Cao, Z. Zhong, W. Fei, J. Feng, *Adv. Sci.* **2019**, 6, 1900246.

- [54] L. Ji, J. Wang, X. Teng, T. J. Meyer, Z. Chen, *ACS Catal.* **2019**, *10*, 412.
- [55] L. Huang, D. Chen, G. Luo, Y. R. Lu, C. Chen, Y. Zou, C. L. Dong, Y. Li, S. Wang, *Adv. Mater.* **2019**, *31*, 1901439.
- [56] L. An, J. Feng, Y. Zhang, R. Wang, H. Liu, G. Wang, F. Cheng, P. Xi, *Adv. Funct. Mater.* **2019**, *29*, 1805298.
- [57] B. Liu, Y. Wang, H. Q. Peng, R. Yang, Z. Jiang, X. Zhou, C. S. Lee, H. Zhao, W. Zhang, *Adv. Mater.* **2019**, *30*, 1803144.
- [58] G. Kresse, J. Hafner, *Phys. Rev. B* **1993**, *47*, 558.
- [59] J. P. Perdew, K. Burke, M. Ernzerhof, *Phys. Rev. Lett.* **1996**, *77*, 3865.
- [60] J. Heyd, G. E. Scuseria, M. Ernzerhof, *J. Chem. Phys.* **2003**, *118*, 8207.